ACS APPLIED MATERIALS & INTERFACES

Research Article

www.acsami.org

Novel Silver Nanoparticle–Manganese Oxyhydroxide–Graphene Oxide Nanocomposite Prepared by Modified Silver Mirror Reaction and Its Application for Electrochemical Sensing

Wushuang Bai, Fei Nie, Jianbin Zheng,* and Qinglin Sheng

Institute of Analytical Science, Shaanxi Provincial Key Laboratory of Electroanalytical Chemistry, Northwest University, Xi'an, Shaanxi 710069, China

Supporting Information

ABSTRACT: A gas/liquid interface will be formed when the free volatilized methyl aldehyde gas begins to dissolve in to solution. On the basis of the traditional silver mirror reaction, silver nanoparticle–manganese oxyhydroxide–graphene oxide (Ag-MnOOH-GO) nanocomposite was synthesized at the gas/liquid interface without any protection of inert gas at room temprature. The morphology of the nanocomposites could be controlled by adjusting the reaction temperature and time. The morphology and composition of the nanocomposites were characterized by scanning electron microscopy, transmission electron microscopy, X-ray diffraction, and Fourier transform infrared spectroscopy. The composites were then applied for electrochemical sensing. The electrochemical investigation for the sensor indicates that it has excellent property to catalyze H_2O_2, and could detect H_2O_2 with a low detection limit of 0.2μM and wide linear range of 0.5 μM to 17.8 mM. The present study provides a general platform for the controlled synthesis of nanomaterials and can be extended to other optical, electronic, and magnetic nanocompounds.

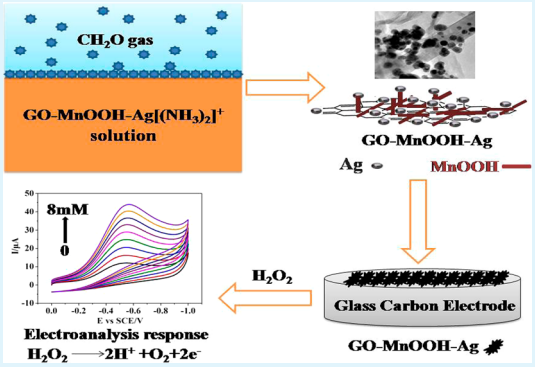

KEYWORDS: *silver mirror reaction, hydrogen peroxide sensor, silver nanoparticles, graphene oxide, MnOOH*

1. INTRODUCTION

As we all know, nanomaterials usually possess large surface areas and exhibit high surface concentrations of edges, corners, defect sites, and other unusual structural features.[1] During the past few decades, much attention has been focused on the synthesis of nanomaterials because of the fundamental significance and promising application in optical, electronic, optoelectronic, and electrochemical nanodevices. Morphology of nanomaterial is an important factor that can influence its properties, so the synthesis of materials with controlled size, orientation, and morphology is one of the most challenging issues with the state of the art.[2]

Nowadays, with the development of nanotechnology, more and more methods have been developed to synthesize nanomaterials, such as chemical and physical precipitation,[3] high-pressure hydrothermal synthesis,[4] sol–gel method,[5] template methods,[6] radiation method,[7] ionic liquid method,[8,9] and electrochemical synthesis.[10−13] Among all the methods, interfacial reaction, such as liquid/liquid and gas/liquid interfacial reactions, based on the chemical reactions that happen at the interface of two different phases, is a special method different from others. The materials synthesized by interfacial reactions also have unique properties; as such, interfacial reaction can be used to control the synthesis of nanomaterials effectively.[14] Rao et al.[15] and Hélder et al.[16] have prepared nanocrystalline films of gold (Au), sliver (Ag), and copper (Cu) based on a toluene/water interfacial reaction. Lee et al.[17] have reported a liquid/liquid interfacial reaction to synthesize Au nanoparticles nanocomposite film which has good properties. Ekarat et al.[18] also have prepared polyaniline (PANI) at a kind of water/organic interface. However, a liquid/liquid interface is not easily manipulated. Compared with the liquid/liquid interfacial reaction, a gas/liquid interface can be easily fabricated, and the reaction can be controlled by adjusting the reaction temperature, the gas pressure, the velocity of gas flow, and throughput. In other words, the size and morphology of nanomaterials that are synthesized by the gas/liquid interfacial reaction can be effectively controlled.

Among all the nanomaterials, silver nanoparticles (AgNPs) receive enormous current research attention. Because of the highest electrical conductivity, antibacterial properties, and excellent catalytic properties, AgNPs have been explored traditionally to employ as catalysts in various chemical, physical, and biological reactions.[19] Therefore, the synthesis of AgNPs has been greatly impressed by a considerable number of researchers. Historically, the silver mirror reaction has been and

Received: November 6, 2013
Accepted: March 24, 2014
Published: March 24, 2014

Scheme 1. (A) Experimental Procedure and (B) Schematic Illustration for the Preparation of Ag-MnOOH-GO Nanocomposites

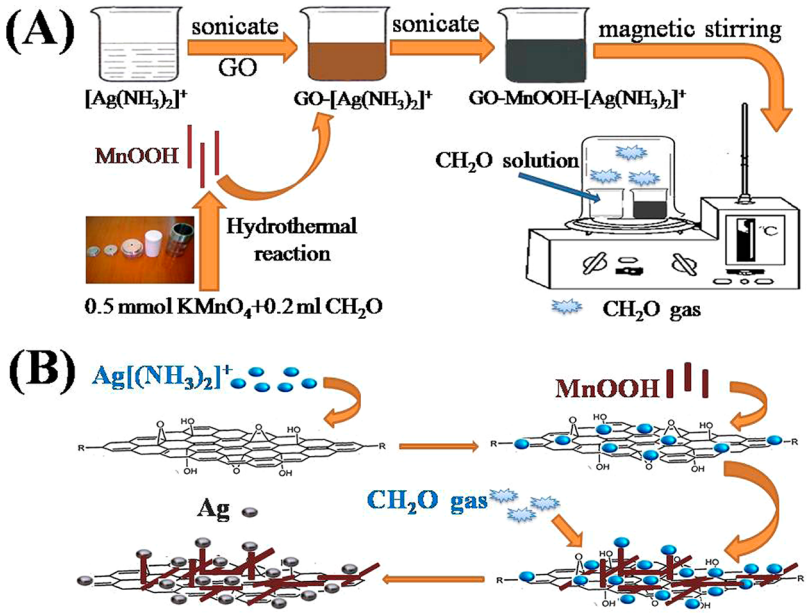

is still being used as an efficient method for preparing thin film coatings of AgNPs.[20] As a convenient and practical method, the silver mirror reaction can obviously produce much smaller homogenized silver particles with narrow size distribution.[21−25] Shan et al.[21] have prepared AgNPs by a silver mirror reaction. The AgNPs loaded on micrometer-size TiO_2, nanosize TiO_2, and $BiVO_4$ have homogenized size and the fabricated Ag/semiconductor photocatalytic composites have perfect properties. Shen et al.[22] have fabricated superhydrophobic surfaces with nanostructures via the silver mirror reaction. By carefully controlling the deposition time, the authors finally obtained a superhydrophobic silver film with high reflectivity, which is as high as that of a polished silicon wafer, and a water contact angle of 174°. ON the basis of the silver mirror reaction, Saito et al.[23] have prepared silver surfaces that show significantly greater surface-enhanced Raman scattering signals than the surface made by the conventional method.

However, because of heating in the water bath and direct addition of the reducing agent solution, the reaction can't stay in control for the fast reaction speed. Because of the advantages of liquid/gas interfacial reaction, it will be a break through to conduct the silver mirror reaction at a liquid/gas interface. As a kind of good reducing agent, methyl aldehyde (CH_2O) can just run off at room temperature and provides a platform to realize the purpose at liquid/gas interface.

In traditional silver mirror reaction, glass plates have been used extensively as the substrates for AgNP growth. Almost no attention has been paid to explore the possibilities of other new surfaces for the formation of silver nanostructures. The appearance of graphene oxide (GO) provides an opportunity to replace the traditional glass substrate. Recently, GO, the oxidized form of graphene, has attracted much attention because of its distinct physical performances such as photoluminescence,[26] ferromagnetism,[27] electrodes,[28] and water permeation.[29] The distinct properties are derived from its unique chemical structure that is composed of segregated sp^2 carbon domains among sp^3 carbons presenting various functional groups.[30] Because of these large numbers of functional groups, many metal nanoparticals can be attached better on the surface of GO. Meanwhile, the hybrid can avoid the self aggregation of GO and nanoparticals effectively.[31] As an efficient strategy, the hybridization of GO with nanoparticles can enhance the electronic, catalytic, and optical properties.[32] To our surprise, we have observed good silver nanostructures produced from the classical silver mirror reaction by changing the glass plate substrate to GO nanosheet with the reducing agent of CH_2O gas. The large amounts of synthesized AgNPs have homogeneous dimension and distribute uniformly on the surface of GO nanosheets.

In this paper, we report results of the studies relating to preparation of Ag-GO and Ag-MnOOH-GO nanocomposites via a modified silver mirror reaction and its application for electrochemical detection of H_2O_2. In contrast with the vast work focusing on synthesis and electrocatalytic application of MnO_2 and Mn_3O_4, reports on the solution phase synthesis of MnOOH are rather rare, and little attention has been paid to their electrochemical characterization. Compared with MnO_2, MnOOH has the better properties to catalyze H_2O_2: it can lower detection limit, enhance the sensitivity, and extend the linear detection range of sensors.[33] Therefore, electrochemical study of MnOOH nanomaterials is necessary and will probably lead to some interesting new finds. In addition, Wang et al.[34] have synthesized GO-MnOOH nanocomposites successfully by a kind of hydrothermal method. So, combining GO, MnOOH, and AgNPs, and then using it for H_2O_2 catalysis will be further expected. Considering the facile preparation route and excellent experimental results, it is possible for the idea to be widely applied in various fields.

2. EXPERIMENTAL SECTION

Materials. Graphite powder (99.998%, 325mesh, Alfa Aesar), Chitosan (CS, MW 5−6 × 10^5, >90% deacetylation) was purchased from Shanghai Yuanju Biotechnology Co., Ltd (Shanghai, China), H_2O_2 (30%, v/v aqueous solution) was got from Tianjin Tianli Chemistry Reagent Co., Ltd (Tianjin, China), 0.1 M phosphate buffered saline (PBS, pH 7.2). All other reagents and chemicals were of analytical reagent grade. Doubly distilled water was used in experiments.

Characterization. Scanning electron microscopic (SEM) measurements were carried out on a scanning electron microscope (JSM-6700F JEOL Japan). Transmission electron microscopic (TEM) images were carried out by Tecnai G^2 F20 S-TWIN (FEI, USA). X-ray diffraction (XRD) patterns of the samples were observed by D/MAX-3C (Rigaku Japan). Fourier transform infrared spectroscopy (FTIR) was recorded with TENSIR 27 (Bruker, German).

Electrochemical measurements were carried out in a conventional three-electrode electroanalysis system controlled by EC 550 electrochemical workstation (Gaoss Union Technology Co., Ltd., Wuhan, China) and CHI 660 electrochemical workstation (Shanghai CH Instrument Co. Ltd., China). All electrochemical experiments were conducted at room temperature (25 ± 2 °C).

Preparation of Ag-MnOOH-GO Nanocomposites. GO was synthesized from graphite powder.[35] Exfoliation of GO was achieved by ultrasonication of the dispersion in an ultrasonic bath.

In a typical synthesis of MnOOH nanorods, 0.5 mmol of $KMnO_4$ and 0.2 mL of CH_2O (36 %; w/w) were dissolved in 35 mL of distilled water and transferred into a Teflon-lined stainless steel autoclave of 40 mL capacity. The synthesis was carried out under hydrothermal conditions at the specified temperature of 120 °C for 10 h. The autoclave was then cooled to room temperature naturally. The products were collected by centrifugation at 5000 rpm for 10 min and washed with distilled water and absolute ethanol several times respectively, followed by drying in a vacuum at 50 °C for 12 h.

The Ag-GO nanocomposites were synthesized by a modified silver mirror reaction. Fifty-five microliters of 5% NaOH solution was added into 3 mL of $AgNO_3$ aqueous solution (0.2 %; w/w) until a fine brown precipitate of Ag_2O was formed. Then 6% $NH_3{\cdot}H_2O$ was added into this mixture drop by drop until the precipitate disappeared, and the solution was completely changed to $Ag[(NH_3)_2]^+$. Then 6% $AgNO_3$ solution was added until the solution became pale brown. After 1 drop of 6 % $NH_3{\cdot}H_2O$ was added, the solution became transparent again. Five milligrams of GO was dispersed into this $Ag[(NH_3)_2]^+$ solution, and the mixture was diluted to 50 mL by doubly distilled water and kept on ultrasonic dispersing for 30 min. Then, the mixture and another beaker that had 20 mL of CH_2O solution were put in a closed container. The volatilized CH_2O gas can be used as reductant, and the modified silver mirror reaction was performed for 24 h under room temperature with continuous magnetic stirring.

The Ag-MnOOH-GO nanocomposites were fabricated as Ag-GO, the only difference was that after 5 mg of GO was dispersed into $Ag[(NH_3)_2]^+$ solution, 10 mg MnOOH nanorods were added and kept on ultrasonic dispersing for 30 minutes (Scheme 1).

Preparation of Ag-MnOOH-GO Nanocomposite-Modified Electrode. The glassy carbon electrode (GCE) was prepared by a simple casting method. Prior to use, the GCE was polished with 1.0 and 0.3 μm alumina powder respectively to obtain mirror like surface and rinsed with doubly distilled water, followed by sonication in ethanol solution and doubly distilled water successively. Then, the GCE was allowed to dry in a stream of nitrogen. The composites (1 mg) were kept on ultrasonic dispersing for 30 min in chitosan (1 mL, 0.5%) solution. The obtained suspension (5 μL) was then cast onto the GCE and dried in air at room temperature. The modified electrode can be expressed as Ag-MnOOH-GO/GCE.

Interference Study and Real Sample Analysis. The interference test was carried out by analyzing the amperometric *i-t* response of the Ag-MnOOH-GO/GCE upon the injection of 1 mM H_2O_2 and three common interferences. The interferences selected for the test were 0.1 mM ascorbic acid (AA), 0.1 mM acetaminophen (AP), and 0.1 mM glucose (Glu). The concentrations of the interferences were set according to the average concentration in the human body. The H_2O_2 disinfectant (3% H_2O_2, Xin Rui Da Limited Company, Dezhou China) was used as real samples. Before the experiments, the real samples were diluted with doubly distilled water. The H_2O_2 concentration was detected by the present sensor and the titration method ($KMnO_4$ titration). The three samples were repeated and measured 3 times at −0.2 V, and values were then averaged.

3. RESULTS AND DISCUSSION

Structural and Morphological Studies. Scheme 1 shows the schematic representation for the preparation of Ag-MnOOH-GO nanocomposites. Because of the abundant oxygen-containing functional groups such as hydroxyl, carbonyl, and carboxyl on the GO surface, chemically derived GO nanosheets can be well-dispersed into water to form a homogeneous and stable solution. When the silver ammonia solution was added into the above GO solution, because of electrostatic adsorption, large numbers of $Ag[(NH_3)_2]^+$ ions can be attached on the surface of GO, which is beneficial to the following in situ formation of metallic Ag nanoparticles on the surface of GO nanosheets. After MnOOH was added, it can be adsorbed on the surface of GO. Actually, the interaction between MnOOH and GO may be ascribed to the hydrogen bond.[36] MnOOH nanorods have large numbers of hydroxyls, such as γ-OH and δ-1-OH.[37] Meanwhile, because of the abundant oxygen-containing functional groups on surface of GO, the MnOOH nanorod probably should be adsorbed on the surface of GO based on the hydrogen bond, which can be described as O−H···O. In the presence of these nanorods, the surface of GO becomes rougher, which provides more extra binding sites for the adsorption of $Ag[(NH_3)_2]^+$ ions. The electrostatic adsorption may be attributed to the hydroxyls of MnOOH. Then, in a closed container, as a perfect reducing agent, the volatilized CH_2O gas molecules could be dissolved in the GO-MnOOH-$Ag[(NH_3)_2]^+$ solution easily, and the $Ag[(NH_3)_2]^+$ ions were reduced gradually.

Images A and B in Figure 1 show the TEM patterns of GO and AgNPs-GO. The TEM image of GO (Figure 1A) shows a typical monolayer nanosheet structure, which has a smooth surface with some wrinkles. After the modified silver reaction, large numbers of reduced AgNPs have been attached on the surface of the GO nanosheet (Figure 1B). Compared with other traditional synthetic methods,[38−41] it is seen clearly by the TEM patterns that the AgNPs we synthesized have such advantages: homogeneous particle size, even distribution on the surface of GO without any aggregation, and more adsorption. All of these advantages are beneficial for improving the performance of the Ag-MnOOH-GO sensor. These indicate that the modified silver mirror reaction is an excellent way to synthesize AgNPs on the surface of GO nanosheets.

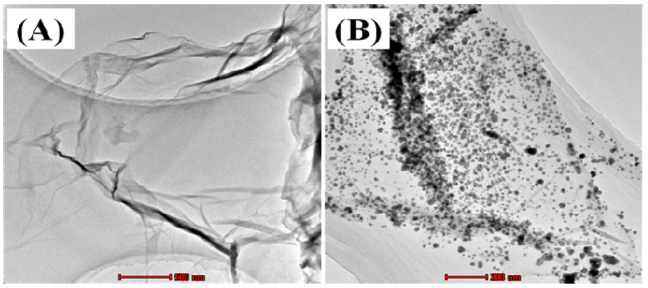

Figure 1. TEM images of (A) GO and (B) Ag-GO nanocomposites.

To research the growth status of AgNPs, we observed the morphologies of AgNPs on GO surface under different reaction times at 298.17 K (Figure 2). The scales of patterns are all 50 nm. At the beginning, Ag nuclei with the size of 5−10 nm are generated when the reaction time is 3 h (Figure 2A). As a result, the average crystallite size becomes larger during the aging process (Figure 2B−D). As shown in Figure 2B, when

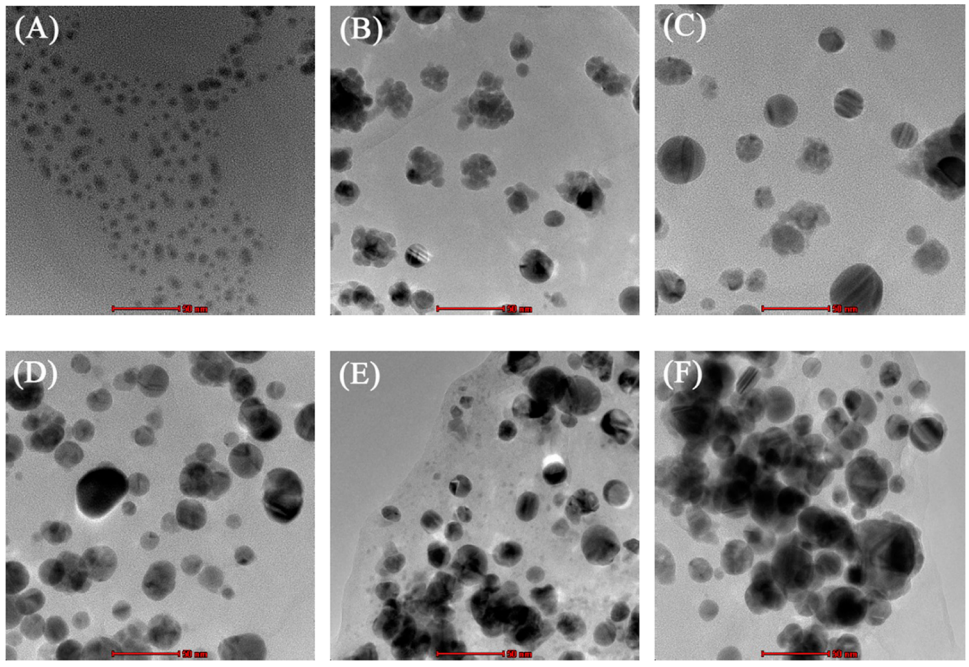

Figure 2. TEM images showing the structural evolution of AgNPs for different reaction durations: (A) 3, (B) 6, (C) 12, (D) 24, (E) 36, and (F) 48 h. The scale bar represents 50 nm.

the reaction time is increased to 6 h, two morphologies are obtained, one is the particle of size 10−20 nm, another like be a kind of aggregation which is composed by many irregular nanosilver of size within 10 nm, we called these half-finished AgNPs. Compared with Figure 2B, more and more particles of size 10−20 nm appear in Figure 2C. It may be because that half-finished AgNPs have grown into particles gradually with continued time. With the reaction time increased to 24 h, the half-finished morphology almost disappeared; instead, larger AgNPs are obtained (Figure 2D). However, when the time is 36 h, some of particles have been aggregated (Figure 2E). With the increase in reaction time to 48 h, the aggregation become more heavily. These indicate that the morphology of AgNPs can be controlled by adjusting the reaction time. In conclusion, the formation of nanoparticles can be composed by two steps: nucleation and growth (Scheme 2). The steps may be presented schematically as reactions 1 and 2,[42] where n is the number of Ag^0 atoms. Nucleation step 1 proceeds homogeneously in solution and involves the reduction of $Ag[(NH_3)_2]^+$ to Ag^0 atoms, followed by their aggregation to the critical nucleus size, $(Ag^0)_n$. As nuclei appear, a fast autocatalytic reduction 2 on the surface of growing particles takes place and limits the rate of their growth.

Scheme 2. Schematic Illustration for the the Formation of AgNPs

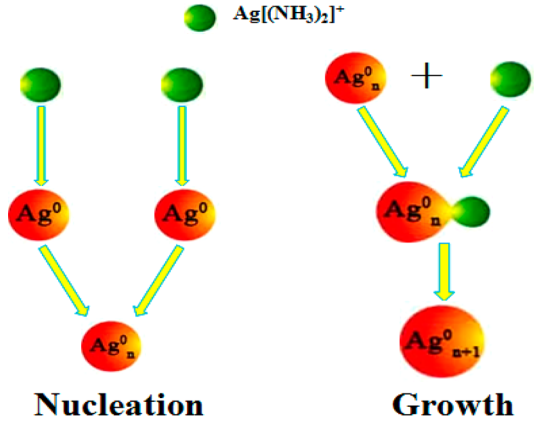

$$nAg[(NH_3)_2]^+ \rightarrow (Ag^0)_n \quad (1)$$

$$(Ag^0)_n + Ag[(NH_3)_2]^+ \rightarrow (Ag^0)_{n+1} \quad (2)$$

Temperature is also one of the most important factors to influence the particles' morphology. Figure 3 shows the TEM images of AgNP-GOs that have been generated under different temperatures with a reaction time of 24 h; the scales of patterns are all 50 nm. The size of particles that are obtained at 298 K is 10−20 nm (Figure 4A), and they are distributed uniformly.

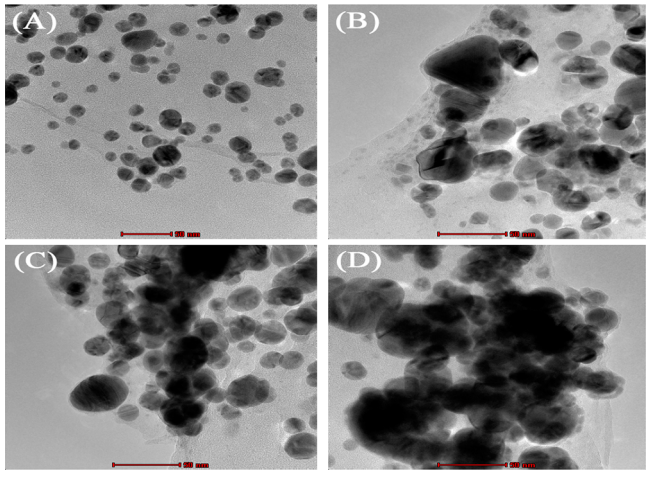

Figure 3. TEM images showing the structural evolution of AgNPs for different reaction temperature: (A) 298, (B) 308, (C) 313, and (D) 318 K. The scale bar represents 50 nm.

dx.doi.org/10.1021/am500641d | ACS Appl. Mater. Interfaces 2014, 6, 5439−5449

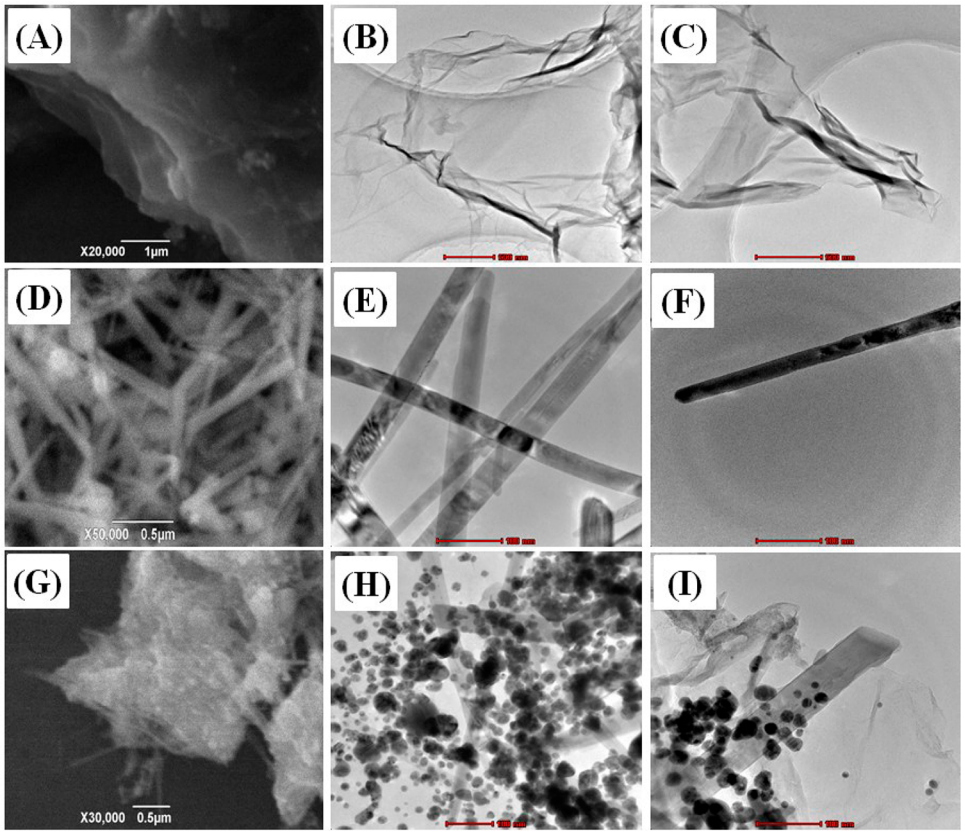

Figure 4. SEM images of (A) GO, (D) MnOOH nanorods and (G) Ag-MnOOH-GO nanocomposites; TEM images of (B, C) GO, (E, F) MnOOH nanorods and (H, I) Ag-MnOOH-GO nanocomposites.

However, when the temperature is increased to 308 K (Figure 3B), the size of the particles increases, and they are agglomerated slightly. As the temperature increases, particles are more heavily agglomerated. As shown in Figure 3C (313 K) and Figure 3D (318 K), the AgNPs are all agglomerated. When the temperature is increased to 318 K, the AgNPs are agglomerated more heavily. These indicate that 298 K is the suitable temperature to synthesize AgNPs and we can also control the morphology by changing the reaction temperature.

Figure 4 show the morphologies of GO, MnOOH, and Ag-MnOOH-GO. As shown in the patterns, we can see the nanorod structure of MnOOH clearly (Figure 4D–F). Their length ranges are several micrometers, and the external diameter is tens of nanometers. It is obviously seen that MnOOH nanorods have been attached on the surface of GO nanosheets, and large numbers of granular nanosilver have been attached on MnOOH nanorods and GO nanosheets (Figure 4G–I).

Furthermore, the XRD patterns of MnOOH nanorods and Ag-MnOOH-GO nanocomposites are shown in Figure 5. As seen from Figure 5A, all of the reflections of the XRD pattern are indexed well to a pure monoclinic phase of γ-MnOOH (manganite, space group $P2_1/c$ (14)) with lattice parameters a = 5.300 Å, b = 5.278 Å, c = 5.307 Å, and β = 114.36° (JCPDS 41-1379). Figure 5B shows the XRD pattern of Ag-MnOOH-GO nanocomposites. It is obviously seen that there are several strong reflection peaks at 2θ values of 38.166, 44.277, and 64.426°, these peaks can be well-indexed to the (111), (200), and (220) planes, respectively (JCPDS 04-0783). Among all peaks, the (111) peak is relatively strong, which indicates the enrichment of the (111) crystalline planes.

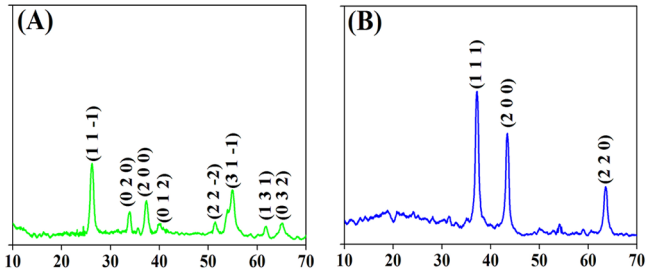

Figure 5. XRD patterns of (A) MnOOH nanorods and (B) Ag-MnOOH-GO nanocomposites.

Figure 6 shows the FTIR spectra of (a) γ-MnOOH, (b) GO, and (c) Ag-MnOOH-GO samples. As shown in Figure 6a, the peaks located at 1083 and 1151 cm^{-1} are attributed to the −OH, respectively, to γ-OH and δ-1-OH.[37] The broad peak at around 2634 cm^{-1} is related to the hydrogen band O−H−, with an O−H···O length of about 2.60 Å in the structure of γ-MnOOH.[43] Another peak at 2041 cm^{-1} could be considered as a combination band of the OH− stretching mode at 2634 cm^{-1} (f_1) and the excited lattice mode at 620 cm^{-1} (f_2). Thus, by $f = f_1 - f_2$, i.e., 2634−620 = 2014 cm^{-1}, the value obtained is very close to the results by Sharma and Kohler.[37] The peaks at 620 and 750 cm^{-1} could be related to the Mn−O vibrations. No other Mn−related vibrations are observed above 800 cm^{-1} in this spectrum, which indicates that the MnOOH nanorods are pure single phase. It is obviously seen that the GO (Figure 6b) shows many strong absorption peaks which are attributed to the various oxygen functional groups. The peak at 3410 cm^{-1} is attributed to the water −OH stretching, the peaks at 1726 and

dx.doi.org/10.1021/am500641d | ACS Appl. Mater. Interfaces 2014, 6, 5439−5449

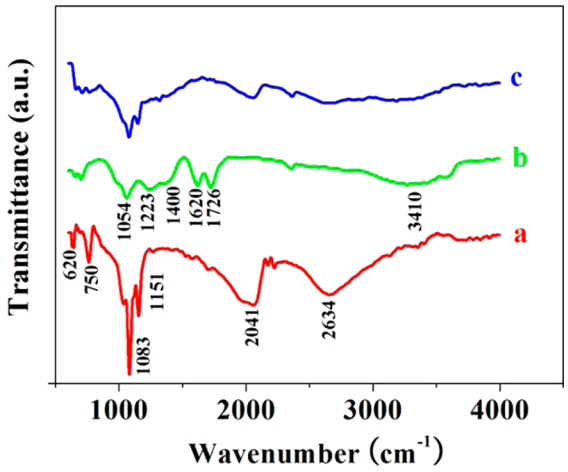

Figure 6. FTIR spectra of (a) MnOOH nanorods, (b) GO, and (c) Ag-MnOOH-GO nanocomposites.

1620 cm^{-1} are related to C═O stretching, water −OH bending, and C═C stretching, respectively, other peaks at 1400,1223, and 1054 cm^{-1} could be attributed to alcoholic C−OH bending, epoxide C−O−C or phenolic C−O−H stretching and C−O stretching, respectively.[44,45] After loading of metallic Ag (Figure 6c) particles, the resultant composites show a low absorption-peak intensity of the functional groups, these may be attributed to the existence of Ag that covered absorption peak of GO and MnOOH.

Electrochemical Properties of Ag-MnOOH-GO Nanocomposites. Electrochemical impedance spectroscopy (EIS) is a powerful tool for studying properties of surface-modified electrodes. Generally, the semicircle diameter equaled to the electron transfer resistance (R_{ct}). According to the relationship between R_{ct} and exchange current density $R_{ct}= (RT)/Fi_0$,[46] the value of R_{ct} decreased after introducing AgNPs and MnOOH-AgNPs into the GO-modified electrode (Figure 7). In the

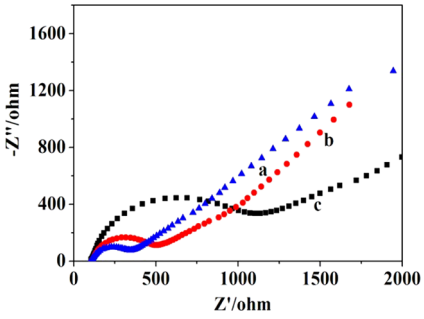

Figure 7. EIS of (a) Ag-GO/GCE, (b) Ag-MnOOH-GO/GCE, and (c) GO/GCE in 5.0 mM $[Fe(CN)_6]^{4-/3-}$ containing 0.1 M KCl from 1×10^5 to 1×10^{-2} Hz at amplitude of 5 mV.

impedance spectra, the value of R_{ct} is decreased from 1000 to 300 Ω after introducing AgNPs into the GO-modified electrode, whereas the value is decreased to 500 Ω after introducing MnOOH and AgNPs. These results suggest that after GO was modified on GCE, electron transfer between the solution and the electrode is less efficient which is ascribed to the presence of less-conductive GO, when Ag is immobilized onto the electrode, the electron transfer resistance value is reduced because of the good conductivity of AgNPs that decreased the impedance of the electrode. Because of the semiconduction of MnOOH nanorods, the Ag-MnOOH-GO electrode is less conductive than the Ag-GO electrode. In general, AgNPs could efficiently enhance the electron transfer efficiency.

The electrochemical behavior of the obtained materials at different stages was investigated with CV, and the results are shown in Figure 8. It is obviously seen that in N_2-saturated 0.1 M PBS (pH 7.2), GO, Ag-GO, MnOOH-GO, and Ag-MnOOH-GO (curve a, c, e, f respectively) exhibit almost no electrochemical response in the absence of H_2O_2. However, after adding 1.0 mM H_2O_2, the electrochemical responses are increased with varying degrees. In contrast, GO (curve b) shows no significant current response, whereas Ag-MnOOH-GO (curve f) shows a remarkable catalytic current peak about 18 μA in intensity at −0.55 V. Compared with Ag-GO (curve d) and MnOOH-GO (curve g), the peak current of Ag-MnOOH-GO is increased about 5 and 10 μA, respectively, which may be attributed to the synergistic effect of MnOOH and AgNPs. MnOOH nanorods provide extra surface for adsorption, and then more adsorbent AgNPs improve the catalytic performance. All the above observations indicate that AgNPs contained in the nanocomposites exhibit a notable catalytic performance for H_2O_2 reduction.

As AgNPs could efficiently enhance the electron transfer efficiency for this hybrid material, therefore, the amount of AgNPs and MnOOH in the hybrid materials may be an important factor to obtain the material with the best electrocatalytic property. We have synthesized such Ag-MnOOH-GO composites with different amount of AgNPs and MnOOH, and then fabricated different sensors for H_2O_2 detection. As seen in panels A and C in Figure 9, with the increase of AgNPs, the H_2O_2 current responses are also aggrandized. However, when 7 mL of $AgNO_3$ was added in the synthetic process, the obtained Ag-MnOOH-GO composite has lower analytical performance instead. This may be because that too many AgNPs have been aggregated, and catalytic performance of the composite has been affected deeply. In addition to these, curves b and c almost have the same highest current response, which indicates that whether 5 or 3 mL of $AgNO_3$ was added, the composites we obtained almost have the same catalytic performance; economically, 3 mL of $AgNO_3$ is more appropriate. Also, the amount of MnOOH in the hybrid materials is an important factor affecting the performance of the composite. As seen in panels B and D in Figure 9, more and more MnOOH has been added in the hybrid materials, and the current responses increase with it. But when 20 mg of MnOOH was added, the current response becomes lower. As we all know, MnOOH is semiconductive; electrons will be impeded in the presence of too many MnOOH nanorods. Therefore, 15 mg of MnOOH is more appropriate.

According to the literature,[47] the mechanism of H_2O_2 electroreduction can be expressed as follows

$$H_2O_2 + e^- \rightleftharpoons OH_{(ad)} + OH^- \quad (3)$$

$$OH_{(ad)} + e^- \rightleftharpoons OH^- \quad (4)$$

$$2OH^- + 2H^+ \rightleftharpoons 2H_2O \quad (5)$$

When the AgNPs are deposited on the electrode, the reaction become more irreversible

$$H_2O_2 \xrightarrow{Ag} \frac{1}{2}O_2 + H_2O \quad (6)$$

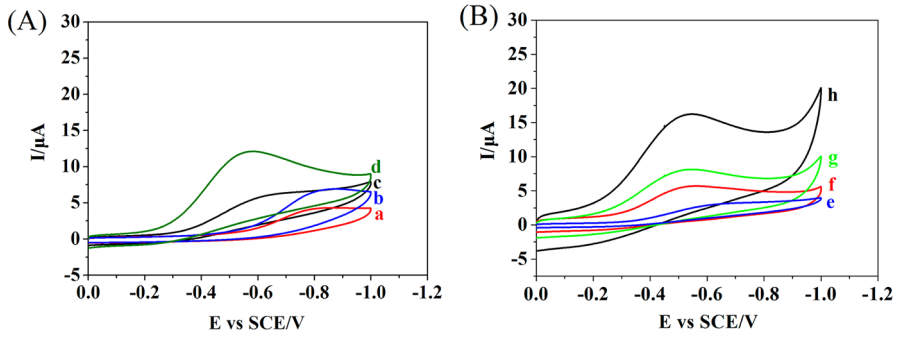

Figure 8. (A) CVs of (a, b) GO/GCE and (c, d) Ag-GO/GCE, as well as (B) CVs of(e, g) MnOOH-GO/GCE and (f, h) Ag-MnOOH-GO/GCE in N_2-saturated 0.1 M PBS (pH 7.2) in the (a, c e, f) absence and (b, d g, h) presence of 1 mM H_2O_2 at a scan rate of 50 mV/s.

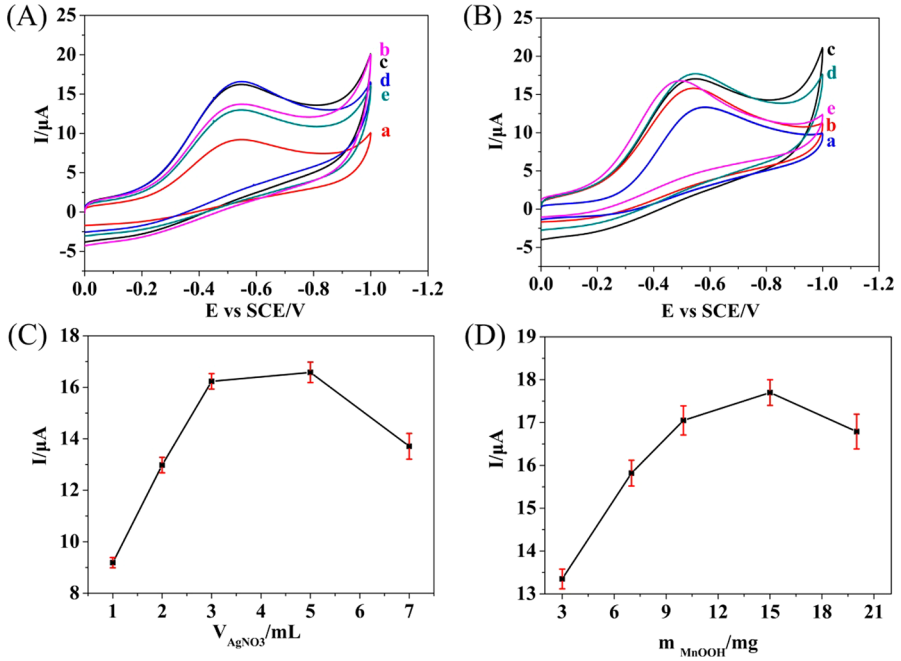

Figure 9. (A) CVs showing the current responses of Ag-MnOOH-GO/GCE with different amount of AgNPs: (a) 1, (b) 2, (c) 3, (d) 5, and (e) 7 mL $AgNO_3$ aqueous solution (0.2 %; w/w) as well as (B) CVs showing the current responses of Ag-MnOOH-GO/GCE with different amount of MnOOH: (a) 3, (b) 7, (c) 10, (d) 15, and (e) 20 mg in N_2-saturated 0.1 M PBS (pH 7.2) containing 1 mM H_2O_2 at a scan rate of 50 mV/s. (C) Highest current response values of Ag-MnOOH-GO/GCE with different amounts of AgNPs as well as (D) the highest current response values of Ag-MnOOH-GO/GCE with different amounts of MnOOH.

Then the O_2 generated in the action above would turn into the detection signal on electrode. It have been proposed that the electroreduction of oxygen on electrode occurred via the mechanism shown below[48]

$$O_2 + e^- \rightleftharpoons [O_2^{\cdot -}]_{(ads)}$$

$$[O_2^{\cdot -}]_{(ads)} + H_2O \rightleftharpoons HO^{\cdot}_{2(ads)} + OH^- \quad (8)$$

Then

$$HO^{\cdot}_{2(ads)} + O_2^{\cdot -} \rightleftharpoons HO^-_{2(aq)} + O_2 \quad (9)$$

or

$$HO^{\cdot}_{2(ads)} + e^- \rightleftharpoons HO^-_{2(aq)} \quad (10)$$

When AgNPs are used as catalysts, the reduction of H_2O_2 become more completely and the detection signal of H_2O_2 will be amplified.

The catalytic responses of the Ag-MnOOH-GO nanocomposite-modified electrode by changing the concentration of H_2O_2 are shown in Figure 10A. It can be seen that in N_2-saturated 0.1 M PBS (pH 7.2), with the increase in H_2O_2 concentration, the highest reduction current responses gradually increased because of the excellent electrocatalytic activity of Ag-MnOOH-GO nanocomposites. Figure 10B shows the calibration curves of catalytic current versus H_2O_2 concentration. A good linear relationship is found between the catalytic current and H_2O_2 concentration at a range from 0 to 8 mM (R = 0.9994). Figure 10C shows the corresponding CV curves of the Ag-MnOOH-GO electrode under different scan rates. As shown in Figure 10D, the peak current shows linear dependence on the square root of the scan rate and obeys the Randles−Sevcik equation $i_p = 0.4463n^{3/2}F^{3/2}AD_{app}{}^{1/2}Cv^{1/2}/(RT)^{1/2}$. In this equation, n is the electron transfer number, F is Faraday's constant, R is the gas constant (8.314 J mol^{-1} K^{-1}), T is the room temperature (298.15 K in our case), A is the area of the GCE, D_{app} is the apparent electron diffusion coefficient, C is the effective electroactive site concentration, and v is the scan rate.[49] By plotting i_p vs $v^{1/2}$ (Figure 9D), the $D_{app}{}^{1/2}C$ can be

dx.doi.org/10.1021/am500641d | ACS Appl. Mater. Interfaces 2014, 6, 5439−5449

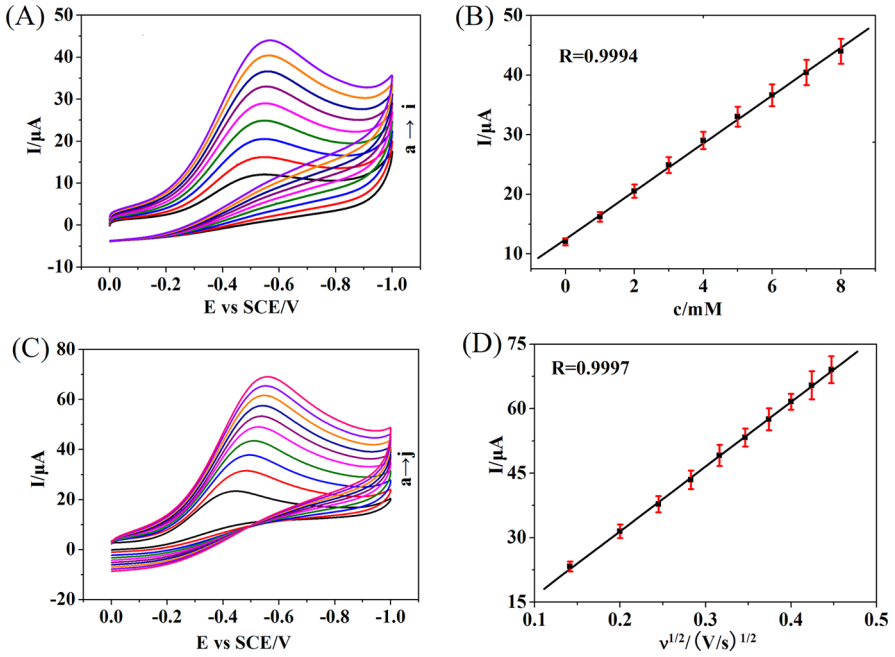

Figure 10. (A) CVs of Ag-MnOOH-GO/GCE in N_2-saturated 0.1M PBS (pH 7.2) in the absence and presence of H_2O_2 with different concentrations (from a to i: 0, 1, 2, 3, 4, 5, 6, 7, and 8 mM) at a scan rate of 50 mV/s. (B) Linear fitting program of the reduction peak currents with the H_2O_2 concentrations. (C) CVs of Ag-MnOOH-GO/GCE in N_2-saturated 0.1 M PBS (pH 7.2) containing 5 mM H_2O_2 at different scan rates (from a to j: 20, 40, 60, 80, 100, 120, 140, 160, 180, and 200 mV/s). (D) Linear fitting program of the reduction peak currents with the square root of scan rate.

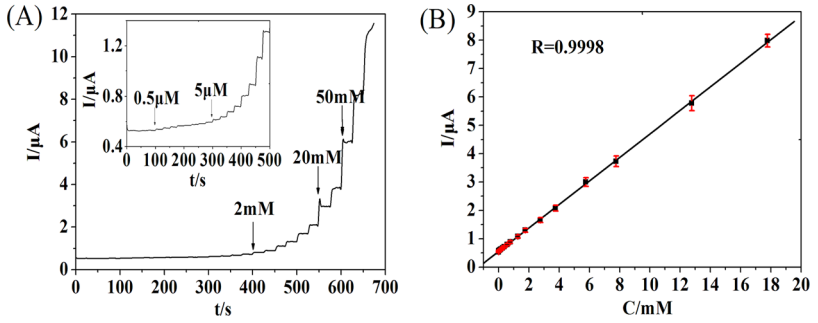

Figure 11. (A) Typical amperometric response of the Ag-MnOOH-GO/GCE on successive injection of H_2O_2 into the stirring N_2-saturated 0.1 M PBS (pH 7.2), applied potential: −0.2 V. (B) Calibration curve of H_2O_2 versus its concentration.

Table 1. Comparison of Several Typical Nonenzymatic and Enzymatic H_2O_2 Sensors

sensors	applied potential (V)	response time (s)	linear range (mM)	sensitivity (μA mM^{-1} cm^{-2})	detection limit (μM)	literature
Ag/MWCNTs/gold electrode	−0.2	5	0.05−17	20.0	0.5	51
Ag NPs/F-SiO_2/GO/GCE	−0.3	2	0.1−260		4	52
MnO_2/GO/GCE	−0.3	5	0.005−0.6	38.2	0.8	53
MnO_2/carbon fiber microelectrode	+0.58		0.012−0.26	10.6	5.4	54
Hb/CNTPME	−0.8	7	0.21−0.9		9.0	55
Ag-MnO_2- MWCNTs/GCE	−0.3	2	0.005−10.4	82.5	1.7	50
Ag NPs/rGO/GCE	−0.3	2	0.1−100		3.6	56
MnO_2/OMC/GCE	+0.45		0.0005−0.6		0.07	57
MnOOH/GCE	−0.3		0.00015−1.6		0.15	33
Ag-MnOOH-GO/GCE	−0.2	3	0.0005−17.8	59.1	0.2	this work

estimated. C in the film can be calculated from the surface coverage and the film thickness.[37] Because of the good linear relationship between the catalytic current and square root of the scan rate (R = 0.9997), an accurate value of D_{app} can be obtained, that is, the apparent electron diffusion of Ag-MnOOH-GO electrode can be controlled.

Figure 11A shows the amperometric response of Ag-MnOOH-GO nanocomposites modified GCE in N_2-saturated 0.1 M PBS (pH 7.2) for the different concentration of H_2O_2. Although the modified electrode exhibits biggest catalytic activity at about −0.5 V, determination of the H_2O_2 was carried out at −0.2 V, such a potential can ensure the lower

background, good signal-to-noise ratio and less interference of other electroactive species in the solution, also, the oxygen reduction current can be limited.[50] Here, Ag-MnOOH-GO nanocomposites modified GCE shows the amperometric current response for H_2O_2 within 3 s, indicating a fast response behavior. Figure 11B shows the calibration curve of the sensor. The linear detection range is from 0.5 μM to 17.8 mM with a correlation coefficient of 0.9998, the sensitivity is 59.14 μA mM^{-1} cm^{-2} and the detection limit is estimated to be 0.2 μM at a signal-to-noise ratio of 3. Compared to our previous work, the H_2O_2 sensor herein has improved the detection limit and the linear range, especially the broad linear range. Moreover, the performance comparisons of the present sensor with others are presented in Table 1. Through these comparisons, obviously, performances of the Ag-MnOOH-GO/GCE are better than that of other electrodes, especially the extremely wide linear range, the low detection limit and the short response time. The wide linear range and low detection limit may be due to the unique structure and performances of Ag-MnOOH-GO nanocomposites. In the composite, GO play a role as a template. Because of the abundant oxygen-containing functional groups, large numbers of homogeneous AgNPs can be attached on the surface of GO nanosheets by the modified silver mirror reaction. After MnOOH nanorods are added, they provid extra superficial area to attach more AgNPs. So, more electroactive sites can be obtained for H_2O_2 adsorption and reaction. The short response time may be due to the high electron transfer rate of AgNPs, otherwise, the uniform size of AgNPs is in favor of fast electron transfer.

To investigate the selectivity and anti-interference advantages of the modified electrode, the interference effects have been investigated by comparing the amperometric responses of Glu, AA, AP (0.1 mM, respectively) with H_2O_2 (1 mM) on the modified electrode in N_2-saturated 0.1 M PBS (pH 7.2) at a working potential of −0.2 V.[51] As shown in Figure S1A in the Supporting Information, the Ag-MnOOH-GO/GCE exhibits good ability of anti-interference to these distractions. The interfering species of oxygen have been also investigated by testing the amperometric responses of H_2O_2 at −0.2 V. As seen from Figure S1B in the Supporting Information, the electrode exhibits good ability of anti-interference to O_2. These properties may be attributed to the unique anti-interference ability of Ag-MnOOH-GO composites, and the relatively lower potential of −0.2 V can limit the reduction of these distractions.

Real Sample Analysis and the Stability of Sensor. To verify the reliability of the sensor, we detected the H_2O_2 concentration in the real sample of disinfectant. The determination results are summarized in Table S1 in the Supporting Information. The results indicate that it is enough to limit the interference effects for real sample analysis, the sensor could be used for H_2O_2 samples analysis and the sensor also has good repeatability. The stability of Ag-MnOOH-GO/GCE ware also evaluated, and results showed that the Ag-MnOOH-GO/GCE has good stability (see Table S2 in the Supporting Information).

4. CONCLUSION

In summary, Ag-MnOOH-GO nanocomposites have been synthesized at a gas/liquid interface based on traditional silver mirror reaction. By adjusting the reaction time and temperature, we can obtain the AgNPs of different size and morphology successfully. The Ag-MnOOH-GO/GCE obtained in this work has been successfully employed as a H_2O_2 sensor which shows a low detection limit of 0.2 μM and particularly wide linear range of 0.5 μM to 17.8 mM. We believe that the procedure to synthesize Ag-MnOOH-GO nanostructures can be considered a general approach and can be extended to other optical, electronic, and magnetic nanocompounds, enabling the development of high-performance electrochemical sensors. Further works derived by the idea in our research for nanomaterials synthesis are on our schedule.

■ ASSOCIATED CONTENT

Ⓢ Supporting Information

The selectivity and anti-interference advantages of the Ag-MnOOH-GO/GCE, the real sample analysis and the reproducibility and stability of Ag-MnOOH-GO/GCE. This material is available free of charge via the Internet at http://pubs.acs.org.

■ AUTHOR INFORMATION

Corresponding Author

*E-mail: zhengjb@nwu.edu.cn. Tel. & Fax: +86 29 88303448.

Notes

The authors declare no competing financial interest.

■ ACKNOWLEDGMENTS

The authors gratefully acknowledge the financial support of this project by the National Science Fund of China (21275116), Specialized Research Fund for the Doctoral Program of Higher Education (No. 20126101120023), the Natural Science Fund of Shaanxi Province in China (2012JM2013, 2013JM2006), the Fund of Shaanxi Province Educational Committee of China (12JK0576), the Scientific Research Foundation of Shaanxi Provincial Key Laboratory (2010JS088, 11JS080, 12JS087, 13JS097) and the Graduate Innovation Fund of Northwest University (YZZ12019).

■ REFERENCES

(1) Soreta, T. R.; Strutwolf, J.; Henry, O.; O'Sullivan, C. K. Electrochemical Surface Structuring with Palladium Nanoparticles for Signal Enhancement. *Langmuir* **2010**, *26*, 12293−12299.

(2) Han, L.; Xiong, P.; Bai, J. F. Spontaneous Formation and Characterization of Silica Mesoporous Crystal Spheres with Reverse Multiply Twinned Polyhedral Hollows. *J. Am. Chem. Soc.* **2011**, *133*, 6106−6109.

(3) Zhao, Y. Y.; Fan, H. M.; Li, W. Incorporation of Polyoxotungstate Complexes in Silica Spheres and in Situ Formation of Tungsten Trioxide Nanoparticles. *Langmuir* **2010**, *26*, 14894−14900.

(4) Chen, J.; Li, C.; Zhao, D. W. A Quantum Dot Sensitized Solar Cell Based on Vertically Aligned Carbon Nanotube Templated ZnO Arrays. *Electrochem. Commun.* **2010**, *12*, 1432−1435.

(5) Akpan, U. G.; Hameed, B. H. The Advancements In Sol−Gel Method of Doped-TiO_2 Photocatalysts. *Appl. Catal., A* **2010**, *375*, 1−11.

(6) Takahashi, Y.; Tatsuma, T. Electrodeposition of Thermally Stable Gold and Silver Nanoparticle Ensembles Through a Thin Alumina Nanomask. *Nanoscale* **2010**, *2*, 1494−1499.

(7) Liu, F. K.; Huang, P. W.; Chu, T. C. Gold Seed-Assisted Synthesis of Silver Nanomaterials Under Microwave Heating. *Mater. Lett.* **2005**, *59*, 940−944.

(8) Duan, X. C.; Lian, J. B.; Ma, J. M. Shape-Controlled Synthesis of Metal Carbonate Nanostructure via Ionic Liquid-Assisted Hydrothermal Route: The Case of Manganese Carbonate. *Cryst. Growth Des.* **2010**, *10*, 4449−4455.

(9) Sheng, Q. L.; Liu, R. X.; Zheng, J. B. Prussian Blue Nanospheres Synthesized in Deep Eutectic Solvents. *Nanoscale* **2012**, *4*, 6880−6886.

(10) Chu, D. W.; Masuda, Y.; Ohji, T. Shape-Controlled Growth of $In(OH)_3/In_2O_3$ Nanostructures by Electrodeposition. *Langmuir* **2010**, *26*, 14814−14820.
(11) Sokolov, S.; Paul, B.; Ortel, E. Template-Assisted Electrostatic Spray Deposition as a New Route to Mesoporous, Macroporous, and Hierarchically Porous Oxide Films. *Langmuir* **2011**, *27*, 1972−1977.
(12) Lucky, R. A.; Yaocihuatl, M. G.; Paul, A. C. Zr Doping on One-Dimensional Titania Nanomaterials Synthesized in Supercritical Carbon Dioxide. *Langmuir* **2010**, *26*, 19014−19021.
(13) Shin, D. O.; Lee, D. H.; Moon, H. S. Sub-Nanometer Level Size Tuning of a Monodisperse Nanoparticle Array Via Block Copolymer Lithography. *Adv. Funct. Mater.* **2011**, *21*, 250−254.
(14) Chowdhury, D.; Paul, A.; Chattopadhyay, A. Macroscopic and Mesoscopic Patterns Observed in Thin Films Formed due to Polymerization of Aniline at the Air−Water Interface. *J. Colloid Interface Sci.* **2003**, *256*, 70−76.
(15) Rao, C. N. R.; Kulkarni, G. U.; Agrawal, V. V. Films of Metal Nanocrystals Formed at Aqueous-Organic Interfaces. *J. Phys. Chem. B* **2003**, *107*, 7391−7395.
(16) Hélder, A. S.; Chirea, M.; Vladimir, G. M. Electrochemical Study of Interfacial Composite Nanostructures: Polyelectrolyte/Gold Nanoparticle Multilayers Assembled on Phospholipid/Dextran Sulfate Monolayers at a Liquid-Liquid Interface. *J. Phys. Chem. B* **2005**, *109*, 20105−20114.
(17) Lee, K. Y.; Cheong, G. W.; Han, S. W. C_{60}-Mediated Self-assembly of Gold Nanoparticles at the Liquid/Liquid Interface. *Colloids Surf., A* **2006**, *275*, 79−82.
(18) Ekarat, D.; Stephan, T. D. Interfacial Polymerization of Water-Soluble Polyaniline and Its Assembly Using the Layer-By-Layer Technique. *J. Met., Mater. Miner.* **2009**, *19*, 39−44.
(19) Sun, Y. G.; Xia, Y. N. Shape-Controlled Synthesis of Gold and Silver Nanoparticles. *Science* **2002**, *298*, 2176−2179.
(20) Qu, L. T.; Dai, L. M. Novel Silver Nanostructures from Silver Mirror Reaction on Reactive Substrates. *J. Phys. Chem. B* **2005**, *109*, 13990.
(21) Shan, Z. C.; Wu, J. J.; Xu, F. F. Highly Effective Silver/Semiconductor Photocatalytic Composites Prepared by a Silver Mirror Reaction. *J. Phys. Chem. C* **2008**, *112*, 15423−15428.
(22) Shen, L. Y.; Ji, J.; Shen, J. C. Silver Mirror Reaction as an Approach to Construct Superhydrophobic Surfaces with High Reflectivity. *Langmuir* **2008**, *24*, 9962−9965.
(23) Saito, Y.; Wang, J. J.; Smith, D. A.; Batchelder, D. N. A Simple Chemical Method for the Preparation of Silver Surfaces for Efficient SERS. *Langmuir* **2002**, *18*, 2959−2961.
(24) Li, X. Y.; Shen, J.; Du, A. Facile Synthesis of Silver Nanoparticles with High Concentration via a CTAB-induced Silver Mirror Reaction. *Colloids Surf., A* **2012**, *400*, 73−79.
(25) Xu, Z. H.; Hao, J. M.; Li, F. S. Surface-Enhanced Raman Spectroscopy of Arsenate and Arsenite Using Ag Nanofilm Prepared by Modified Mirror Reaction. *J. Colloid Interface Sci.* **2010**, *347*, 90−95.
(26) Loh, K. P.; Bao, Q.; Eda, G.; Chhowalla, M. Graphene Oxide as a Chemically Tunable Platform for Optical Applications. *Nat. Chem.* **2010**, *2*, 1015−1024.
(27) Wang, Y.; Huang, Y.; Song, Y.; Chen, Y. Room-Temperature Ferromagnetism of Graphene. *Nano Lett.* **2009**, *9*, 220−224.
(28) Miller, J. R.; Outlaw, R. A.; Holloway, B. C. Graphene Double-Layer Capacitor with ac Line-Filtering Performance. *Science* **2010**, *329*, 1637−1639.
(29) Nair, R. R.; Wu, H. A.; Jayaram, P. N. Unimpeded Permeation of Water through Helium-Leak-Tight Grapheme-Based Membranes. *Science* **2012**, *335*, 442−444.
(30) Bagri, A.; Mattevi, C.; Acik, M. Structural Evolution During the Reduction of Chemically Derived Graphene Oxide. *Nat. Chem.* **2010**, *2*, 581−587.
(31) Williams, G.; Seger, B.; Kamat, P. V. TiO_2-Graphene Nanocomposites UV-Assisted Photocatalytic Reduction of Graphene Oxide. *ACS Nano* **2008**, *2*, 1487−1491.
(32) Scheuermann, G. M.; Rumi, L.; Steurer, P. Palladium Nanoparticles on Graphite Oxide and Its Functionalized Graphene Derivatives as Highly Active Catalysts for the Suzuki-Miyaura Coupling Reaction. *J. Am. Chem. Soc.* **2009**, *131*, 8262−8270.
(33) Cao, X.; Wang, N.; Wang, L. A Novel Non-Enzymatic Hydrogen Peroxide Biosensor Based on Ultralong Manganite MnOOH Nanowires. *Sens. Actuators, B* **2010**, *147*, 730−734.
(34) Wang, L.; Wang, D. L. Preparation and Electrochemical Characterization of MnOOH Nanowire-Graphene Oxide. *Electrochim. Acta* **2011**, *56*, 5010−5015.
(35) Luo, G. Q.; Jiang, X. J.; Li, M. Facile Fabrication and Enhanced Photocatalytic Performance of Ag/AgCl/rGO Heterostructure Photocatalyst. *ACS Appl. Mater. Interfaces* **2013**, *5*, 2161−2168.
(36) Chen, S.; Zhu, J. W.; Wu, X. D. Graphene Oxide MnO_2 Nanocomposites for Supercapacitors. *ACS Nano* **2010**, *4*, 2822−2830.
(37) Sharma, P. K.; Whittingham, M. S. The Role of Tetraethyl Ammonium Hydroxide on the Phase Determination and Electrical Properties of γ-MnOOH Synthesized by Hydrothermal. *Mater. Lett.* **2001**, *48*, 319−323.
(38) Shen, J. B.; Shi, M.; Yan, B. One-Pot Hydrothermal Synthesis of Ag-Reduced Graphene Oxide Composite with Ionic Liquid. *J. Mater. Chem.* **2011**, *21*, 7795−7801.
(39) Xu, C.; Wang, X. Fabrication of Flexible Metal-Nanoparticle Films Using Graphene Oxide Sheets as Substrates. *small* **2009**, *5*, 2212−2217.
(40) Chen, P.; Yin, Z. Y.; Huang, X. Assembly of Graphene Oxide and $Au_{0.7}Ag_{0.3}$ Alloy Nanoparticles on SiO_2: A New Raman Substrate with Ultrahigh Signal-to-Background Ratio. *J. Phys. Chem. C* **2011**, *115*, 24080−24084.
(41) Xu, W. P.; Zhang, L. C.; Li, J. P. Facile Synthesis of Silver@ Graphene Oxide Nanocomposites and Their Enhanced Antibacterial Properties. *J. Mater. Chem.* **2011**, *21*, 4593−4597.
(42) Watzky, M. A.; Finke, R. G. Transition Metal Nanocluster Formation Kinetic and Mechanistic Studies. A New Mechanism When Hydrogen Is the Reductant: Slow, Continuous Nucleation and Fast Autocatalytic Surface Growth. *J. Am. Chem. Soc.* **1997**, *119*, 10382−10400.
(43) Zhang, W. X.; Yang, Z. H.; Liu, Y. Controlled Synthesis of Mn_3O_4 Nanocrystallites and MnOOH Nanorods by a Solvothermal Method. *J. Cryst. Growth* **2004**, *263*, 394−399.
(44) Li, Q.; Guo, B. D.; Yu, J. G. Highly Efficient Visible-Light-Driven Photocatalytic Hydrogen Production of CdS-Cluster-Decorated Graphene Nanosheets. *J. Am. Chem. Soc.* **2011**, *133*, 10878−10884.
(45) Shen, J.; Li, T.; Long, Y.; Shi, M.; Li, N.; Ye, M. One-Step Solid State Preparation of Reduced Graphene Oxide. *Carbon* **2012**, *50*, 2134−2140.
(46) Mano, N.; Mao, F.; Heller, A. Characteristics of a Miniature Compartment-less Glucose-O_2 Biofuel Cell and Its Operation in a Living Plant. *J. Am. Chem. Soc.* **2003**, *125*, 6588−6594.
(47) Masataka, H.; Takuro, K.; Hideaki, K. Electrochemical Behavior of H_2O_2 at Ag in $HClO_4$ Aqueous Solution. *Electrochim. Acta* **1986**, *31*, 377−383.
(48) Xu, J.; Huang, W. H. Isotope and Surface Preparation Effects on Alkaline Dioxygen Reduction at Carbon Electrodes. *J. Electroanal. Chem.* **1996**, *410*, 235−242.
(49) Wang, J. Y.; Chen, L. C.; Ho, K. C. Synthesis of Redox Polymer Nanobeads and Nanocomposites for Glucose Biosensors. *ACS Appl. Mater. Interfaces* **2013**, *5*, 7852−7861.
(50) Han, Y.; Zheng, J. B.; Dong, S. Y. A Novel Nonenzymatic Hydrogen Peroxide Sensor Based on Ag-MnO_2-MWCNTs Nanocomposites. *Electrochim. Acta* **2013**, *90*, 35−43.
(51) Zhao, W.; Wang, H. C.; Qin, X. A Novel Nonenzymatic Hydrogen Peroxide Sensor Based on Multi-Wall Carbon Nanotube/Silver Nanoparticle Nanohybrids Modified Gold Electrode. *Talanta* **2009**, *80*, 1029−1033.
(52) Lu, W. B.; Luo, Y. L.; Chang, G. H. Synthesis of Functional SiO_2-Coated Graphene Oxide Nanosheets Decorated with Ag Nanoparticles for H_2O_2 and Glucose Detection. *Biosens. Bioelectron.* **2011**, *26*, 4791−4797.

(53) Li, L. M.; Du, Z. F.; Liu, S. A Novel Nonenzymatic Hydrogen Peroxide Sensor Based on MnO_2/Graphene Oxide Nanocomposite. *Talanta* **2010**, *82*, 1637−1641.
(54) Hocevar, S. B.; Ogorevc, B.; Schachl, K. Glucose Microbiosensor Based on MnO_2 and Glucose Oxidase Modified Carbon Fiber Microelectrode. *Electroanalysis* **2004**, *16*, 1711−1716.
(55) Zhao, Y. D.; Bi, Y. H.; Zhang, W. D. The Interface Behavior of Hemoglobin at Carbon Nanotube and the Detection for H_2O_2. *Talanta* **2005**, *65*, 489−494.
(56) Li, Z. Q.; Qin, X. Y.; Luo, Y. L. One-Pot Synthesis of Ag Nanoparticles/Reduced Graphene Oxide Nanocomposites and Their Application for Nonenzymatic H_2O_2 Detection. *Electrochim. Acta* **2012**, *83*, 283−287.
(57) Luo, L. Q.; Li, F.; Zhu, L. M. Non-Enzymatic Hydrogen Peroxide Sensor Based on MnO_2-ordered Mesoporous Carbon Composite Modified Electrode. *Electrochim. Acta* **2012**, *77*, 179−183.